The Aluminum-in-Olivine Thermometer for Mantle Peridotites - Experimental versus Empirical Calibration and Potential Applications

Y. Bussweiler*[a], G. P. Brey[b], D. G. Pearson[a], T. Stachel[a], R. A. Stern[a], M. F. Hardman[a], B. A. Kjarsgaard[c], S. E. Jackson[c]

[a)] Department of Earth and Atmospheric Sciences, University of Alberta, 126 ESB, Edmonton, AB T6G 2E3, Canada

[b)] Institut für Geowissenschaften, FE Mineralogie, Johann Wolfgang Goethe-Universität Frankfurt, Altenhöferallee 1, 60438 Frankfurt, Germany

[c)] Geological Survey of Canada, 601 Booth Street, Ottawa, ON, Canada K1A 0E8

*Corresponding author at: Department of Earth and Atmospheric Sciences, University of Alberta, 126 ESB, Edmonton, AB T6G 2E3, Canada. Tel.: +1 780 492 3265; Fax: +1 780 492 2030. E-mail address: bussweil@ualberta.ca (Y. Bussweiler)

Abstract

This study provides an experimental calibration of the empirical Al-in-olivine thermometer for mantle peridotites proposed by De Hoog et al. (2010). We report Al concentrations measured by secondary ion mass spectrometry (SIMS) in olivines produced in the original high-pressure, high-temperature, four-phase lherzolite experiments by Brey et al. (1990). These reversed experiments were used for the calibration of the two-pyroxene thermometer and Al-in-orthopyroxene barometer by Brey and Köhler (1990). The experimental conditions of the runs investigated here range from 28 to 60 kbar and 1000 to 1300 °C. Olivine compositions from this range of experiments have Al concentrations that are consistent, within analytical uncertainties, with those predicted by the empirical calibration of the Al-in-olivine

thermometer for mantle peridotites. Fitting the experimental data to a thermometer equation, using the least squares method, results in the expression:

$$T\,[°C] = (11245 + 46.0 * P\,[kbar]) / (13.68 - \ln(Al\,[ppm])) - 273$$

This version of the Al-in-olivine thermometer appears to be applicable to garnet peridotites (lherzolites and harzburgites) well outside the range of experimental conditions investigated here. However, the thermometer is not applicable to spinel-bearing peridotites. We provide new trace element criteria to distinguish between olivine from garnet-, garnet-spinel-, and spinel-facies peridotites. The estimated accuracy of the thermometer is ±20 °C. Thus, the thermometer could serve as a useful tool in settings where two-pyroxene thermometry cannot be applied, such as garnet harzburgites and single inclusions in diamond.

Keywords

Aluminum; Olivine; Thermometry; Experimental Calibration; Garnet Peridotite; Kimberlite

1. Introduction

Olivine and its high-pressure polymorphs dominate the mineralogy of Earth's upper mantle and transition zone (e.g., Ringwood, 1966; Stachel et al., 2005). Despite its overwhelming presence in the mantle cargo of kimberlites, thus far, olivine has played only a minor role in diamond exploration efforts. Meanwhile, other, much less abundant minerals, occurring in till samples and concentrate from kimberlite, such as garnet and clinopyroxene, are routinely used in diamond exploration as indicator minerals. These minerals have proved to be crucial in finding kimberlite occurrences and, more importantly, in helping to assess the diamond potential of a kimberlite pipe (e.g. Gurney 1984; Schulze 1997; Grütter et al. 2004). Recent studies have shown that the majority of olivine in kimberlite may originate from disaggregated mantle xenoliths (e.g., Kamenetsky et al. 2008; Brett et al. 2009; Arndt et al. 2010; Bussweiler et al. 2015). Moreover, in Arctic regions, such as the Slave Craton, olivine is well preserved, even in till

samples. Thus, in these settings olivine has great potential in exploration as an indicator mineral, with an especially promising application being the Al-in-olivine geothermometer.

While the incorporation of Al in olivine appears to be dominantly controlled by T, a variety of substitution and exchange mechanisms are operative in different settings (De Hoog et al. 2010, and references therein). Thus, different expressions of the thermometer are required, for example, for magmatic and mantle olivines. Among mantle olivines, the different facies (garnet-, spinel-, or garnet-spinel) may further play an important role in element partitioning. As the olivine paragenesis cannot always be determined from the sample context, i.e. for single grains from till or concentrate, developing reliable olivine trace element screens is of great importance.

The empirical calibration of the Al-in-olivine thermometer for mantle peridotites by De Hoog et al. (2010) is based on Al concentrations measured by laser ablation inductively coupled mass spectrometry (LA-ICP-MS) in olivines from natural mantle xenoliths derived from different volcanic rock types, including kimberlites and alkali basalts, from a variety of locations and tectonic settings. In combination with P and T estimates from other geothermobarometers, namely the two-pyroxene thermometer and Al-in-orthopyroxene barometer (Brey and Köhler, 1990), an expression of T as a function of P and a compositional term, Cr/(Cr+Al) (Cr#), was obtained:

$$T_{Al\text{-}Ol}\,[°C] = (9423 + 51.4*P\,[kbar] + 1860*Cr\#) / (13.409 - \ln Al\,[ppm]) - 273 \qquad \text{Eqn. 1}$$

(De Hoog et al., 2010)

Although only olivines from garnet lherzolites were used in deriving this calibration, the thermometer was found to be applicable to garnet harzburgites and garnet-spinel lherzolites as well (De Hoog et al., 2010). A strength of this calibration is that samples with natural Al abundances were used, and that the T calibration range is large, ~800 to 1400 °C, effectively spanning much of the mantle sampling window of kimberlites. A disadvantage of any empirical thermometer is, however, that it critically depends on the accuracy of the geothermobarometers used for the independent P and T estimates (Canil, 1999). Thus far,

no independent experimental calibration of this thermometer exists, in contrast to its lower-P, magmatic analog, based on the exchange of Al between olivine and Cr-spinel (Coogan et al., 2014; Wan et al., 2008).

A simplified equation, based on an earlier version of the empirical calibration (De Hoog and Gall, 2005), has been proposed by Korolyuk and Pokhilenko (2014), albeit without an estimate of the applicable range of conditions or the resulting uncertainties in the estimated T. Such a simplified equation would have great potential as a single-crystal thermometer in settings where other indicator minerals, such as pyroxenes and garnet, are rare to absent. Another important example of application is single olivine inclusions in diamond.

In this study, we focus on the accuracy of the empirical calibration of the Al-in-olivine thermometer from an experimental perspective. We revisit the original experiments used for the calibration of the two-pyroxene thermometer and Al-in-orthopyroxene barometer (Brey and Köhler, 1990) and measure Al directly in the experimentally-equilibrated olivines by SIMS. We then present a calibration of the Al-in-olivine thermometer based on the precisely known experimental P and T conditions, and compare the results with the empirical version of the thermometer. We test the applicability of our experimental calibration to natural samples by comparison to the two pyroxene thermometer and the Ca-in-orthopyroxene thermometer by Brey and Köhler (1990), and the single-clinopyroxene thermometer by Nimis and Taylor (2000).

The use of SIMS in this study is necessary due to the need for high spatial resolution and high analytical sensitivity, given that olivines in the experimental runs are usually < 30 μm in size, with Al concentrations of usually < 200 ppm. Moreover, a minimally-destructive approach was preferred in order to preserve the experimental charges for future work.

2. Samples

The experiments used here were performed by Brey et al. (1990) on fertile natural lherzolite compositions over a P range of 10 to 60 kbar and a T range of 900 to 1400 °C. The reversed experiments were performed in a piston cylinder apparatus (for P ≤ 28 kbar) and in a belt apparatus (for P > 28 kbar). Importantly, the experimental conditions are very precisely known, T to ±7 °C and P to ±1% (relative) (Brey et al., 1990). Different starting materials were used in the experiments, with their bulk compositions approximating primitive upper mantle. The mineral compositions of each starting material differed, so that equilibrium mineral compositions could be inferred from overlap of microprobe analyses. Starting materials considered in the present study are 1) mineral mix 'SC-1', which constitutes handpicked mineral separates (olivine, orthopyroxene, clinopyroxene, and spinel) of spinel lherzolite SC-1 (Jagoutz et al., 1979), 2) mineral mix 'J4', which constitutes magnetic separates of orthopyroxene-, clinopyroxene-, and garnet-porphyroclasts from the sheared garnet lherzolite nodule J4 from Jagersfontein, South Africa, combined with olivine from either J4 or from spinel lherzolite Mog 32, and 3) oxide mix 'SCS', which constitutes a synthetic mix of sintered pure oxides (SiO_2, TiO_2, Al_2O_3, Cr_2O_3, MnO, NiO, and MgO) and carbonates ($CaCO_3$ and Na_2CO_3) together with synthetic fayalite to match the SC-1 composition. In two out of 14 cases, the starting composition could not be reliably identified in this study, due to loss of sample material and/or documentation to the original dataset.

3. Methods

Restoration and preparation of the experimental samples and secondary ion mass spectrometry (SIMS) were carried out at the Canadian Centre for Isotopic Microanalysis (CCIM), University of Alberta. All original experimental run products were extracted from their existing epoxy mounts and re-assembled into four new 25 mm diameter epoxy discs (mount numbers M1348, M1349, M1350, M1351). In-house olivine reference materials were also included in the new assemblies. The surfaces were polished lightly with diamond compounds on rotary equipment to create a uniformly flat surface, cleaned with a lab soap solution and de-ionized H_2O, and then coated with 7 nm of high-purity Au prior to scanning electron

microscopy (SEM). Detailed SEM imaging using a backscattered electron detector was carried out utilizing a Zeiss EVO MA15 instrument with beam conditions of 20 kV and 3 – 4 nA. A further 23 nm of Au was subsequently deposited on the mounts prior to SIMS analysis.

Al concentrations were determined from $^{27}Al^-/^{29}Si^-$ ratios in olivine using the IMS-1280 multi-collector ion microprobe at the CCIM. Primary beam conditions utilized 20 keV $^{133}Cs^+$ ions focused to a diameter of 8 μm and a beam current of 0.5 nA. The normal incidence electron gun was utilized for charge compensation. No analytical advantage was found in measuring $^{27}Al^+/^{29}Si^+$ utilizing an O^- primary beam, and the Cs probe was preferred due to the comparative ease of working at small beam diameters with high beam density. Scanning ion imaging of $^{27}Al^-$ preceded many analyses to aid the placement of analytical spots and to avoid overlap with adjacent high-Al minerals such as garnet (see Supplementary Material S1 for images). The primary beam was rastered across a 15 x 15 μm area for 30 s prior to analysis, to clean the surface of Au and contaminants, and to implant Cs. Negative secondary ions were extracted through a 10 kV potential into the secondary column (Transfer section). Conditions for the Transfer section included an entrance slit width of 100 μm, field aperture of 3 x 3 mm, and a field aperture-to-sample magnification of 200 x. Automated tuning of the secondary ions in the Transfer section preceded each analysis. The energy slit was fully open. Both $^{27}Al^-$ and $^{29}Si^-$ were analyzed simultaneously, utilizing a large-format electron multiplier and a Faraday cup, respectively (EM and H'2 using 10^{11} Ω amplifier). The only significant isobar for $^{27}Al^-$ in olivine is $^{26}MgH^-$ and requires a nominal mass resolution of ~3000 to resolve. Although olivine is nominally anhydrous, adsorbed hydrogen is ubiquitous on the mounts and becomes ionized when electron charge compensation is employed. The $^{26}MgH^-$ count rate is generally similar to or lower than that of $^{27}Al^-$, and therefore well-resolved using the working mass resolution > 3500 while maintaining a flat-topped peak scan. Mass scans comparing $^{26}MgH^-$ in Mg-rich and Fe-rich olivine are consistent with its identity. Similarly, for $^{29}Si^-$ the only interference is a weak $^{28}SiH^-$ signal, requiring a mass resolution of ~3400. Separation of $^{29}Si^-$ from the hydride was achieved by using a combination of a larger exit slit (500 μm) and offsetting the peak center to lower mass to allow a wider

flat top than possible with the available fixed exit slits. Examples of mass scans are shown in Supplementary Material S1. The secondary ion count rates for $^{27}Al^-$ and $^{29}Si^-$ in an Fe-rich olivine reference material (Fo12) were both found to be significantly lower (~1/3) than those of Mg-rich olivine (Fo90) with the same Al (and Si) content, indicating a matrix effect. Nevertheless, the Al/Si ratio remained constant, showing that this ratio is a robust proxy for Al concentration in olivine over a wide range of olivine Fo composition.

Mean count rates for $^{27}Al^-$ were in the range 10^2 to 10^4 c/s, and for $^{29}Si^-$ were > 10^6 c/s, determined over a 75s total counting interval for each analysis. The analytical protocol interspersed analyses of unknowns with regular analyses of an olivine xenocryst SC-GB from San Carlos (CCIM primary reference material S0355) with an average Al concentration of 86 ±3 ppm (based on EPMA, LA-ICP-MS and solution-ICP-MS, Supplementary Material S1). A mean $^{27}Al^-/^{29}Si^-$ was determined for each analytical session (one for each mount), and used along with the Al concentration of SC-GB to determine the session sensitivity factor to calculate Al concentrations in unknowns. Only insignificant systematic changes in $^{27}Al^-/^{29}Si^-$ in the primary reference material were observed during a session. Uncertainties in Al concentration propagate within-spot counting errors, the uncertainty in the mean $^{27}Al^-/^{29}Si^-$ for the session, and a blanket spot-to-spot uncertainty of 1.0 ‰ in the $^{27}Al^-/^{29}Si^-$. The total uncertainties (95% confidence) in [Al] per spot , excluding those associated with the absolute abundance of Al in the primary reference material, are generally in the range ±3% to ±10%.

4. Results

A total of 14 experimental charges produced in seven runs (Table 1) were chosen for SIMS analysis. The selected samples show textural evidence for equilibrium, such as equigranular crystals with common 120° grain boundary intersections (Fig. 1). Grain sizes for olivine and other phases range from 5 to 30 µm. Brey et al. (1990) describe a dependency of grain size on the type of starting material (smaller for synthetic mixtures) and temperature (larger for higher T). Based on only small variations in Mg# (±0.3,

165 1σ) in all experiments, Brey et al. (1990) concluded that olivines are generally well-equilibrated in the
166 experiments.

167 Al concentrations were measured by SIMS for up to 10 different olivine grains per experiment. The data
168 were carefully screened for analytical overlap with surrounding high-Al minerals. This could be done
169 based on the analytical uncertainties associated with the measured Al concentrations, given that
170 "contaminated" concentrations are usually associated with higher uncertainties (> 10%). Additionally,
171 post-SIMS BSE images recorded for each analytical spot were checked visually to exclude the possibility
172 that neighboring phases were sampled during analysis. The complete dataset of screened analyses is
173 shown in Table 2.

174 The observed ranges of Al concentrations in olivines within individual experiments can be relatively large
175 (up to 50 ppm, Table 2, Fig. 2), whereas the Mg# of the olivines was found to be more narrowly defined
176 (Brey et al., 1990). This observation can be attributed to the slower diffusion of Al^{3+} compared to divalent
177 atoms, Mg and Fe, in olivine (e.g., Spandler and O'Neill 2010).

178 In order to obtain an equilibrium value from the observed ranges in Al for a particular set of P and T
179 conditions, the overlap in Al concentration for runs using different starting materials was used, following
180 the procedure outlined by Brey et al. (1990). The high analytical precision of SIMS allows us to constrain
181 the overlap range and the associated midpoint reliably (Fig. 2). The midpoint of the overlap range was
182 taken as the equilibrium value, and the maximum analytical uncertainty of the two data points
183 constraining the overlap range was adopted as the uncertainty of the equilibrium value (2σ).

184 For cases where only one starting material was available, i.e. where no midpoints could be determined
185 from compositional overlap (see 50 kbar data plotted in Fig. 2), the mean of the measured range
186 (weighted by the uncertainties of the individual data points) was used as the equilibrium value. The
187 greater analytical uncertainty of the group of data points was assigned as the uncertainty of the
188 equilibrium value (2σ).

189 The resulting equilibrium Al concentrations and their uncertainties for the different runs (i.e. fixed P-T
190 condition) are shown in Fig. 2 and listed in Table 3.

191 Cr was not measured in the experimental olivines during this study. However, Brey (1989) reported Cr_2O_3
192 average concentrations for the different experimental runs (equilibrium values) from electron probe
193 microanalysis (EPMA). Using these published values and the measured Al equilibrium values from this
194 study, the Cr# for all experiments could be calculated (Table 3).

195 ## 5. Discussion

196 The calculated equilibrium Al concentrations from the experiments were compared against the Al
197 concentrations expected from the empirical calibration by De Hoog et al. (2010) in ln (Al) versus 1000/T
198 space (Fig. 3). De Hoog et al. (2010) suggested that the empirical calibration is most reliable for olivines
199 with Cr# between 0.35 and 0.75. The equilibrium Al values from the experiments fall consistently within
200 this empirical range for all experimental P and T (Fig. 3A). Moreover, inserting the respective Cr# for
201 each run (Table 3) along with experimental P and T into the empirical expression by De Hoog et al.
202 (2010) (Equation 1), yields Al values that are within uncertainty of the measured Al concentrations (Fig.
203 3B). However, we note that the latter is not a completely independent test, as Cr# was calculated with the
204 equilibrium Al concentrations from our measurements.

205 ### 5.1. Experimental Calibrations versus Empirical Calibration

206 The experimental dataset (n = 7, Table 3) was fitted to the expected thermometer equation (e.g., Equation
207 1) following the least squares method (using the Solver function in Excel). By describing the
208 experimental T with the three variables experimental P, ln(Al), and Cr#, the following relationship was
209 obtained:

210 $$T\,[°C] = (14750 + 45.1 * P\,[kbar] - 2831 * Cr\#) / (14.97 - \ln(Al\,[ppm])) - 273 \qquad \text{Eqn. 2}$$

211 Cr#, however, is not a strictly independent variable in this dataset, as it is directly related to Al
212 concentration, and there is a strong negative correlation of Cr# with T (R^2 = 0.89). Moreover, the
213 incorporation of Cr itself into olivine has been found to be related to P and T under common mantle redox
214 conditions (De Hoog et al., 2010). To avoid any detrimental effect of these correlations on statistical
215 regression, we now describe T in terms of only P and Al concentration only, which yields the expression:

216 T [°C] = (11245 + 46.0 * P [kbar]) / (13.68 – ln(Al [ppm]) – 273 Eqn. 3

217 The uncertainties on any calculated temperatures using these equations are dominated by the uncertainties
218 in the equilibrium Al concentrations from the experiments, i.e. the 2σ errors in Table 3. Thus, the
219 extremes of the measured Al concentrations in the experimental olivines were inserted into Equations 2
220 and 3, and also into Equation 1, the empirical calibration by De Hoog et al. (2010), to obtain uncertainty
221 estimates at the 95% confidence level. It should be noted that Equations 1 and 2 are affected by an
222 additional uncertainty associated with the calculation of the Cr# value, which also may be on the order of
223 ±10 °C (assuming an average absolute uncertainty of Cr# of 0.03, based on analytical uncertainties, and
224 multiplying by the coefficient 310.8 of Equation 2). The uncertainties for Equations 1 and 2 were thus
225 doubled to take into account propagation of uncertainties on the Cr# measurement. The resulting
226 maximum uncertainties for Equations 1, 2, and 3 are observed for Run 320b, and amount to ±19, ±17, and
227 ±9 °C, respectively (error bars in Fig. 4). Uncertainties in the experimental conditions were not
228 propagated, but the uncertainty for experimental T of ±7 °C (Brey et al., 1990) becomes relevant when
229 evaluating the accuracy of the thermometers (Fig. 4B).

230 Both expressions derived from the experimental calibration (Equations 2 and 3) as well as the empirical
231 calibration by De Hoog et al. (2010) (Equation 1) reproduce the experimental T closely (Fig. 4A). This
232 underlines the good agreement between empirical and experimental calibration of the Al-in-olivine
233 thermometer. The empirical calibration is consistently within error of at least one of the experimental

234 calibrations. However, the empirical calibration (De Hoog et al. 2010; Equation 1) yields, on average,
235 slightly lower temperatures than the experimental calibrations with a somewhat larger spread (Fig. 4B).

236 In terms of accuracy of the different equations, the average absolute deviations from the experimental T
237 of the mean values of the experimental calibrations are 7 °C for Equation 2, 8 °C for Equation 3, and
238 slightly higher for the empirical calibration (17 °C for Equation 1). Yet, given the uncertainty of ±7 °C for
239 the experimental T, these deviations are small.

240 ## 5.2. Critical Evaluation of Cr# in Experimental Olivines

241 In mantle peridotites, Cr substitutes for Al extensively and if only olivine is analyzed, Cr# in olivine is the
242 best proxy for this substitution (De Hoog et al., 2010). Because the Al-in-olivine thermometer for mantle
243 peridotites presented here constitutes a single-mineral thermometer which ignores any Al variation in the
244 other phases that olivine equilibrates with (i.e., garnet, ±clinopyroxene, ±spinel), the Cr# of olivine is, in
245 principle, a crucial parameter in the Al-in-olivine thermometer equation.

246 Here, Cr# values of the experimental olivines were calculated using the original Cr contents reported by
247 Brey (1989) and the new Al values measured by SIMS (Table 3). When comparing the calculated Cr#
248 values to those of natural samples, some potential limitations become evident (Fig. 5A). Firstly, the range
249 of Cr# in the experimental olivines (~0.50 to 0.63) is relatively restricted compared to that of olivines
250 from typical cratonic garnet peridotites (~0.35 to >0.75; e.g., De Hoog et al. (2010)). Moreover, when
251 comparing the Cr# of olivine to that of coexisting clinopyroxene, it appears that the experiments by Brey
252 et al., (1990) behave differently than natural garnet peridotites in that the experimental olivines are
253 displaced towards higher Cr# (Fig. 5A).

254 The observed displacement of the experimental olivines away from the natural xenolith trend can have
255 various underlying reasons. Firstly, the equilibrium of Cr may not have been fully attained in the
256 experimental olivines, due to the slow diffusion of Cr in olivine (Milman-Barris et al., 2008). Secondly,
257 Na loss (due to the presence of a fluid or melt phase) was reported in the original experiments (Brey et al.,

1990). Not only does Na have an effect on the substitution of Al into olivine (by charge balancing the substitution of Mg^{2+}), but it also influences the incorporation of Al and Cr into clinopyroxene. In fact, Brey et al., (1990) attributed variable Cr/Al ratios in clinopyroxene to Na loss. Thus, we cannot confidently establish whether the observed mismatch in Cr# between experiments and natural samples (Fig. 5A) is due to disequilibrium in olivine or clinopyroxene, or both.

In order to test qualitatively whether Cr# of olivine has an effect on the accuracy of our experimental calibration, we have plotted deviations in temperatures (ΔT) calculated with our Al-in-olivine thermometer (Equation 3) from temperatures calculated with the single-clinopyroxene thermometer of Nimis and Taylor (2000), against the range in Cr# of natural olivines (Fig. 5B). No clear correlation of ΔT with Cr# of natural olivines is evident, but Al-in-olivine temperatures appear to be shifted consistently to higher values. The same holds true when comparing against the orthopyroxene-garnet thermometer of Harley (1984) (Fig. 5C). It should be noted that using the thermometer equation which includes the Cr# term (Equation 2) does not change the observed deviations significantly. The systematically slightly higher temperatures obtained with our Al-in-olivine thermometer equation(s) may thus be a function of Na loss in the original experiments, which could have slightly suppressed the incorporation of Al into olivine.

Finally, it should be noted that the coefficient for Cr# in the experimental thermometer formulation (Equation 2) is negative, whereas the corresponding coefficient in the empirical calibration of De Hoog et al., (2010) (Equation 1) is positive. This highlights that the effect of Cr# in Al-in-olivine thermometry still remains somewhat uncertain. For this reason, and due to the equilibrium issues described above, we advise against the use of Equation 2. Instead, we recommend, for the present time, a formulation without the Cr# term (Equation 3) which also shows a generally better fit when applied to natural samples (see below).

5.3. Applicability of Experimental Calibrations to Natural Samples

In order to test whether the new experimental calibrations (Equations 2 and 3) are also valid for natural samples that have equilibrated at conditions outside of the experimental range, the formulations were applied to the dataset of mantle xenoliths from kimberlites published by De Hoog et al. (2010), and additional data for garnet peridotites derived from kimberlites at Diavik (Mather, 2012) and Somerset Island (Kjarsgaard and Peterson, 1992; Mather et al., 2011) (Table 4). The calculated temperatures were compared to values obtained with the two-pyroxene thermometer of Brey and Köhler (1990), the single-clinopyroxene thermometer of Nimis and Taylor (2000), and the orthopyroxene-garnet thermometer of Harley (1984). For consistency, all temperatures were calculated iteratively in combination with the Al-in-orthopyroxene barometer of Brey and Köhler (1990) and the respective P estimates were inserted into the experimental calibrations of the Al-in-olivine thermometer (Table 4).

Both experimental calibrations of the Al-in-olivine thermometer result in good agreement with the two-pyroxene thermometer, including at temperatures outside the range of experimental conditions used in this study (1000 to 1300 °C; Fig. 6A, B). This is true for the garnet lherzolite samples from the dataset of De Hoog et al. (2010) and our new data for garnet peridotites from Diavik and Somerset Island. Equation 2, the formulation including the Cr# term, however, results in more scatter and overall offset from the 1:1 line towards lower temperatures (Fig. 6A). We thus prefer the formulation without Cr# (Equation 3). Another advantage of this equation is that the uncertainties are potentially reduced as it removes the need for precise and accurate Cr determination in addition to Al.

Our preferred formulation (Equation 3) yields results for olivines derived from garnet lherzolites that show excellent fit with the two-pyroxene thermometer (T_{BKN}) over a temperature range from 850 to 1450 °C (Fig. 6B). For garnet lherzolites, the median absolute deviation of our preferred Equation 3 and T_{BKN} indicates agreement within ~ ±20 °C, i.e. agreement within the respective uncertainties of the thermometers. There is also reasonable agreement with the single-clinopyroxene thermometer (T_{NT}), although Al-in-olivine temperatures fall increasingly above T_{NT} towards lower T (Fig. 6C), which could

306 be a function of Na loss in the experiments (see above). The difference in slope between the two
307 thermometers could also be a function of the barometer used in the iterative calculations; T_{NT} gives best
308 results with the corresponding single-clinopyroxene barometer (Nimis and Taylor, 2000).

309 De Hoog et al. (2010) suggested that the Al-in-olivine thermometer is also applicable to garnet
310 harzburgites. At present there is no reliable thermometer available for garnet harzburgite assemblages that
311 could be used for comparison. The garnet-orthopyroxene Mg-Fe exchange thermometer of Harley (1984)
312 systematically overestimates temperatures at low T (< 1000 °C) and underestimates at high T (> 1100 °C;
313 for full discussion see Brey and Köhler, (1990) and Nimis and Grütter (2010)). On that basis, the key
314 observation in Fig. 6D is that the harzburgitic and lherzolitic samples fall on the same linear array,
315 suggesting that the Al-in-olivine thermometer indeed yields reliable T estimates for garnet harzburgites. A
316 possible Al-exchange reaction in clinopyroxene-free harzburgites could be:

317 $MgAl[AlO_4] + 2\ Mg_2Si_2O_6 \leftrightarrow Mg_3Al_2Si_3O_{12} + Mg_2[SiO_4]$

318 olivine + orthopyroxene ↔ garnet + olivine

319 Below 850 °C, the excellent correlation between Al-in-olivine and pyroxene based thermometry breaks
320 down (Fig. 6). All these low-T samples correspond to xenolith samples that also contain spinel (i.e. spinel
321 and spinel-garnet peridotites). This may suggest that the Al-in-olivine thermometer is not applicable to
322 spinel-bearing samples, including garnet-spinel peridotites. Alternatively, it may relate to a decoupling of
323 Al- and Ca-based thermometers at temperatures where Al diffusion becomes exceedingly slow (e.g.,
324 Spandler and O'Neill, 2010). In the latter case, a simple cut-off at a minimum T of 850 °C for the
325 applicability of the Al-in-olivine thermometer would be sufficient. In the former case, however, the well-
326 established existence of depleted spinel-garnet peridotites (e.g., 5-phase lherzolites) at higher
327 temperatures (and pressures) needs to be considered (Grütter et al., 2006; Klemme, 2004; Ziberna et al.,
328 2013).

In order to distinguish between olivine derived from garnet peridotites, garnet-spinel peridotites, and spinel peridotites, other trace element systematics in olivine can be used. De Hoog et al. (2010) proposed that the different lithologies can be most successfully separated by plotting Zr vs. Sc, and to a lesser extent Al vs. Mn (their Fig. 7), with olivine in garnet peridotites being characterized by higher Zr and lower Sc and Mn.

Here, we recommend Al vs. V as a more robust discriminating plot. V is another T-sensitive element in mantle olivine and thus shows a positive relationship with Al (De Hoog et al., 2010). Moreover, V is strongly compatible with spinel and thus displays lower concentrations in olivine from spinel-bearing lithologies. This leads to distinct trends for the different peridotite facies (Fig. 7). Olivines from garnet-facies peridotites trend towards the highest Al and V concentrations with increasing T (Fig. 7). Olivines from garnet-spinel peridotites have consistently low Al concentrations, often < 10 ppm (Fig. 7). This can be expected to be primarily a function of their lower equilibration temperatures. The modal proportion of spinel in garnet-spinel peridotites is typically very low, usually < 1 vol% (Ziberna et al., 2013), so that the effect on Al partitioning into olivine is likely to be small. Olivines from true spinel peridotites (garnet absent) have higher Al concentrations, and the exchange dominantly occurs between olivine and spinel. The latter exchange mechanism has been exploited for the calibration of the Al-in-olivine thermometer for spinel peridotites and magmatic settings (e.g., Wan et al. 2008; Coogan et al. 2014). An exception to these trace element systematics are olivines that have experienced substantial metasomatism in the mantle, such as those recently reported from the Benfontein sill, South Africa (Howarth and Taylor, 2016). Such olivines have elevated Al, Ca, and Na contents, and thus overlap with olivines from spinel-peridotites in Fig. 7, whereas other discriminating plots place them within the garnet peridotite field (Howarth and Taylor, 2016; their Fig. 8a). Al-in-olivine temperatures calculated for such metasomatized grains are likely to be overestimated. Overall, a combination of facies-discriminating plots can be applied in order to increase the reliability of the Al-in-olivine thermometer.

5.4. The Al-in-Olivine Thermometer as an Exploration Tool?

As for almost all geothermometers, a P estimate is required in order to calculate T with Equation 3, which is problematic when dealing with single olivine grains (e.g, recovered during indicator mineral sampling). We thus suggest a simplified approach in which the Al-in-olivine thermometer may be used without a corresponding P estimate, in order to evaluate the depth of mantle sampling, which is similar to the application of the Ni-in-garnet thermometer (Canil, 1999; Griffin et al., 1989). A realistic example for this simplified approach would be a kimberlite occurrence that is under-explored, for example due to the paucity of other indicator minerals such as garnet, but which is located in a reasonably well-understood setting where the geotherm at the time of kimberlite eruption (paleogeotherm) is known. In such a case, T can be extrapolated to the geotherm to yield P, which can be converted to mantle sampling depth. It should be noted, however, that this method does not take into account possible thermal perturbations, which occur in deep lithospheric mantle sections, associated in particular with hot sheared peridotites.

In practice, a large, random sample of olivine grains should be analyzed for their major element composition (e.g., Mg and Fe to calculate Mg#), minor elements (e.g., Ni, Mn, and Ca), as well as trace elements (e.g., Al and V). Except for V, all of these components are accessible by EPMA, if proper background limits, high probe currents, and long count times are used (e.g., Korolyuk and Pokhilenko, 2014; Sobolev et al., 2007). However, in order to obtain precise Al and V concentrations (down to < 10 ppm) LA-ICP-MS is required. Alternatively, SIMS may be used to maximize spatial resolution and precision. If the goal is to limit the analysis to one method, we recommend that LA-ICP-MS is used (if Si is used as the internal standard, a constant content of ~19.1 wt% can be assumed for olivine). When dealing with mineral mounts that have been polished, it can be assumed that the vast majority of the exposed cores represent mantle xenocrysts, because magmatic overgrowths are usually thin and easily removed. Olivine from mantle peridotites should fulfill the following compositional criteria (e.g., Arndt et al., 2010; Brett et al., 2009; Bussweiler et al., 2015; Foley et al., 2013; Kamenetsky et al., 2008):

1. Mg# ≥ 0.90

2. NiO ≥ 0.3 wt% (~2350 ppm)
3. MnO ≤ 0.15 wt% (~1160 ppm)
4. CaO ≤ 0.1 wt% (~715 ppm)

These screens should exclude magmatic olivine, e.g. in the form of magmatic overgrowths/phenocrysts (Arndt et al., 2010; Brett et al., 2009; Bussweiler et al., 2015; Fedortchouk and Canil, 2004; Howarth and Taylor, 2016; Kamenetsky et al., 2008) and also olivines belonging to the Cr-poor megacryst suite (Moore and Costin, 2016; Moore, 2012). Olivines of the Cr-rich suite, however, have similar composition to lherzolitic olivines (Moore and Costin, 2016) and may, by extension, also yield robust Al-in-olivine temperatures. Moreover, we emphasize that our thermometer equation is most applicable to olivine from cratonic garnet peridotites and their corresponding olivines should have Cr# >0.45 (Fig. 5).

All olivine analyses from our example dataset from Somerset Island (n = 69; see Extended Data) pass the above screens. In order to test whether the olivines come from spinel-, garnet-, or garnet-spinel peridotites, they can be plotted in the Al vs V diagram (Fig. 7). This test is important because the Al-in-olivine thermometer presented in this study (Equation 3) is applicable only to garnet-facies olivines. The Somerset Island data mostly overlap with the garnet-facies field (Supplementary Fig. 1). They are thus suitable for the Al-in-olivine thermometer presented in this study (Equation 3). However, at Al concentrations below ~10 ppm, it becomes difficult to distinguish between olivines from garnet-facies and garnet-spinel-facies peridotites. Thus, to minimize incorrect facies classification, we recommend excluding all data points with < ~10 ppm Al. In our example dataset from Somerset Island, this results in the screening of 14 from 69 analyses (hollow symbols in Fig. 8)

Al-in-olivine temperatures can then be projected onto the geotherm by expressing the latter as a linear equation (solved for P), combining it with Equation 3, and calculating P and T iteratively. For the geotherm projections, simplified equations of the geotherms of Hasterok and Chapman (2011) may be used, or the software package FITPLOT may be applied for more sophisticated fitting equations

(McKenzie et al., 2005; Mckenzie and Bickle, 1988). Here, the first approach was followed, yielding somewhat lower values than published in Mather et al. (2011), e.g. 42 vs. 44 mW/m^2 for Somerset Island.

In Fig. 8A, the projected example olivine dataset from Somerset Island and a smaller (non-statistical) dataset from Diavik (n = 7) are shown. The mantle beneath Diavik is characterized by a cold geotherm (~38 mW/m^2) which usually implies high diamond potential (Grütter, 2009). Here, all of the analyzed Diavik olivines fall within the "diamond window", i.e. below the graphite/diamond boundary (Day, 2012; Kennedy and Kennedy, 1976) before intersecting the mantle adiabat. At Somerset Island, the geotherm is significantly hotter (~42 mW/m^2) so that only a small number of olivines fall within the diamond window. This is in agreement with Somerset Island kimberlites having an extremely low diamond grade of < 1 ct per 100 t (Irvine et al., 2003; Kjarsgaard and Levinson, 2002).

The P-T points, obtained from projecting Al-in-olivine temperatures onto a geotherm, can further be plotted as a histogram. For clarity, P has been converted into depth in km, using a simplified conversion factor of 3.15 (Fig. 8B). The bin size should be chosen to be larger than the uncertainty of the thermometer (~20 °C, which in this example relates to ~3 km depth). Such a probability density plot will provide an estimate of the "mantle sampling behavior" of the transporting magma, i.e. kimberlite. In the example of Somerset Island, the majority of olivines were derived from ~140 km depth. Moreover, the histogram plot allows an estimation of the proportion of olivines that have equilibrated with spinel. In Fig. 8B, the more erratically distributed depths below ~100 km (i.e., Al-in-olivine temperatures < 850 °C), correspond to spinel-bearing samples and are probably not reliable (see above).

Importantly, olivine sampling depth profiles, such as the one obtained for Somerset Island (Fig. 8B), can further be coupled to other compositional parameters, such as Mg# (Fig. 8B), minor and trace elements. Olivine, being the most abundant mineral in the mantle, should yield more reliable results for overall mantle sampling than garnet, which usually constitutes < 10 modal % of mantle peridotite xenoliths. As

425 such, depth profiles obtained from Al-in-olivine thermometry, as presented in this study, provide a
426 powerful tool aiding in the mapping of lithospheric mantle (e.g., Gaul et al., 2000).

427 6. Conclusions

428 Al concentrations measured by SIMS in olivines from the original high-P, high-T experiments by Brey et
429 al. (1990) are in agreement with the empirical calibration of the Al-in-olivine thermometer by De Hoog et
430 al. (2010). Our experimental dataset allows for an independent calibration of the thermometer as a
431 function of Al concentration and pressure. The expression appears to be applicable to olivines from garnet
432 peridotites that have equilibrated over a large P-T range, with an estimated accuracy of ~ ±20 °C. The
433 applicability of the thermometer to garnet harzburgites, in addition to garnet lherzolites, makes the Al-in-
434 olivine thermometer an important tool in mantle studies. Moreover, the Al-in-olivine geothermometer
435 could serve as a useful diamond exploration tool in settings where other indicator minerals are rare.
436 Olivine sampling depth profiles, obtained from projecting Al-in-olivine temperatures onto
437 (paleo)geotherms, can provide an important reference frame for future lithospheric mantle mapping
438 studies.

439 Acknowledgments

440 This study forms part of Y.B.'s Ph.D. research, funded through the Canada Excellence Research Chair
441 awarded to D.G.P. Analytical work for this project was funded through an NSERC Discovery Grant to
442 T.S., and a Society of Economic Geologists Canada Foundation (SEGCF) grant awarded to Y.B. The
443 author is further grateful for a University of Alberta Doctoral Recruitment Scholarship. Kate Hogberg is
444 thanked for help with sample preparation for SIMS. Pedro Waterton is thanked for assistance with
445 solution ICP-MS. Natasha Barrett is thanked for providing olivines from spinel lherzolites (Fiji). The
446 manuscript has benefitted greatly from two very constructive reviews from Paolo Nimis and Cees-Jan De
447 Hoog. We thank Marco Scambelluri for the efficient editorial handling.

Figure Captions

Fig. 1 Backscattered electron (BSE) image of experimental sample S3321A, run P3, at 28 kbar and 1150 °C with starting material J4 (Brey et al., 1990). The sample contains orthopyroxene (opx, dark grey), olivine (ol, grey), garnet (grt, light grey), and clinopyroxene (cpx, light grey with low relief).

Fig. 2 Measured Al concentrations by SIMS versus experimental temperatures, for four different experimental pressures (28, 40, 50, and 60 kbar). Where possible, equilibrium Al values (in blue) for the different runs were constrained from the midpoints of compositional overlap (filled blue circles) of different starting materials. In cases where only one starting material was available (e.g. the lower T runs at 50 kbar), the weighted mean of the measured range was used as the equilibrium value (see text).

Fig. 3 A) ln(Al) versus 1000/T plot, relating equilibrium Al concentrations in olivines from experiments used in this study to the empirical calibration by De Hoog et al. (2010). Contours were calculated with Equation 1, solved for Al and inserting the respective Cr# threshold values (0.35 and 0.75) and pressures. Symbols correspond to Al values measured by SIMS (this study) coded by their respective experimental P and plotted at their respective experimental T. Error bars correspond to 2σ uncertainty in the equilibrium values (see text). B) Same plot without Cr# and P contours, including expected Al concentrations (green symbols) calculated by inserting experimental P, T, and Cr# into the empirical equation by De Hoog et al. (2010).

Fig. 4 A) Temperature versus experimental pressure (not continuous). Dashed grey line represents experimental temperatures (Brey et al., 1990). The experimental calibrations in this study, with Cr# (Equation 2, solid black circles) and without Cr# (Equation 3, open circles), and the empirical calibration by De Hoog et al. (2010) with Cr# of the experimental olivines (Equation 1, green diamonds), all reproduce the experimental T closely. B) Deviation from experimental T in °C at the different experimental P-T conditions. Average absolute deviations are 7 °C for the experimental calibration with

Cr# (Equation 2), 8 °C for the experimental calibration without Cr# (Equation 3), and 17 °C for the empirical calibration by De Hoog et al. (2010) (Equation 1).

Fig. 5 A) Cr# (Cr/[Cr+Al]) of olivine versus Cr# of coexisting clinopyroxene in the experiments of Brey et al. (1990) (open circles) and in natural olivines from garnet peridotite xenoliths from kimberlites (solid diamonds) (De Hoog et al., 2010). The experimental olivines are displaced towards higher Cr#, which may indicate imperfect equilibrium in the experiments (see text). B) Deviations in temperatures (ΔT) calculated with our Al-in-olivine thermometer (Equation 3) from temperatures calculated with the single-clinopyroxene thermometer of Nimis and Taylor (2000) plotted against Cr# of natural olivines from cratonic garnet peridotites. C) Deviations in temperatures (ΔT) calculated with our Al-in-olivine thermometer (Equation 3) from temperatures calculated with the orthopyroxene-garnet thermometer of Harley (1984). Olivine data are from De Hoog et al. (2010) (solid diamonds) and new data from Diavik, Slave Craton (red diamonds) and from Somerset Island, Northern Canada (blue circles) (see Table 4).

Fig. 6 Al-in-olivine temperatures calculated for olivine from different mantle xenoliths from kimberlites (De Hoog et al., 2010) including new data (this study) for garnet peridotites from Diavik (red diamonds) and Somerset Island (blue circles). A) Temperatures calculated with Equation 2 (experimental calibration with Cr#) compared to the two-pyroxene thermometer (Brey and Köhler, 1990), B) Temperatures calculated with Equation 3 (experimental calibration without Cr#) compared to the two pyroxene-thermometer (Brey and Köhler, 1990), C) Temperatures calculated with Equation 3 (experimental calibration without Cr#) compared to the single-clinopyroxene thermometer (Nimis and Taylor, 2000), D) Temperatures calculated with Equation 3 (experimental calibration without Cr#) compared to the orthopyroxene-garnet thermometer (Harley, 1984), including harzburgitic samples from the dataset of De Hoog et al. (2010), from Diavik (Mather, 2012), and from Kimberley (Creighton et al., 2009). The dashed lines represent the ±50 °C interval.

Fig. 7 Al versus V concentration in olivines from different xenolith facies based on data from De Hoog et al. (2010) (diamond-shaped symbols) and from our own database (circle-shaped symbols), including the data from Diavik and Somerset Island (see Table 4 and Supplementary Material S3). The garnet-(spinel-) facies field is dominated by cratonic peridotite xenoliths derived from kimberlites from different locations (e.g., Kaapvaal Craton, Slave Craton, Siberian Craton) and contains more lherzolites than harzburgites. The spinel-facies field is dominated by non-cratonic settings (e.g., Ray Pic, Massif Central, France; San Carlos, Arizona; Fiji). Olivine from garnet-facies peridotites (gt) has high Al and high V. Olivine from garnet-spinel facies peridotites (gt-sp) has consistently low Al (< 10 ppm). Olivine in spinel-peridotites (sp) again has relatively high Al but low V (< 6 ppm). The red crosses represent core analyses of olivines from the Benfontein kimberlite sill, South Africa, that are interpreted to be derived dominantly from garnet peridotites. A sub-group of these cores have experienced Al-enrichment due to mantle metasomatism (Howarth and Taylor, 2016). T contours for the garnet-facies field were calculated by projecting Al-in-olivine temperatures (using Equation 3) onto a cold cratonic geotherm of 38 mW/m^2 (see text).

Fig. 8 A) Al-in-olivine temperatures projected onto geotherms (Hasterok and Chapman, 2011) by iterative calculation (see text). Two example data sets are shown: Diavik olivines fall along a cold geotherm (38 mW/m^2), Somerset Island olivines fall along a hot geotherm (42 mW/m^2). Based on the graphite/diamond transition (Day, 2012), all of the Diavik olivines, but only few Somerset Islands olivines fall within the "diamond window". B) Probability density plot for Somerset Island olivines (n = 69) showing the frequency of olivines derived from a certain depth (or pressure) obtained from projecting Al-in-olivine temperatures onto the geotherm (see text). Such depth profiles applied to a large, random sample (e.g., from heavy mineral concentrates) provide an estimate of the sampling behavior of the transporting magma, i.e. kimberlite. The depth profiles can be coupled to compositional parameters, such as Mg# of olivine, here shown as median value and range (if available). Temperatures < 850 °C (or

518 depths < 100 km) are probably not reliable, but have geological meaning as they can indicate the presence
519 of spinel (see Fig. 6 and 7).

520 References

521 Arndt, N.T., Guitreau, M., Boullier, A.M., Le Roex, A., Tommasi, A., Cordier, P., Sobolev, A., 2010.
522 Olivine, and the origin of kimberlite. J. Petrol. 51, 573–602. doi:10.1093/petrology/egp080

523 Brett, R.C., Russell, J.K., Moss, S., 2009. Origin of olivine in kimberlite: Phenocryst or impostor? Lithos
524 112, 201–212. doi:10.1016/j.lithos.2009.04.030

525 Brey, G.P., 1989. Geothermobarometry for lherzolites: experiments from 10 to 60 kb, new
526 thermobarometers and application to natural rocks. Habilit. Thesis, TU, Darmstadt 227.

527 Brey, G.P., Köhler, T.P., 1990. Geothermobarometry in four phase lherzolites II. New thermobarometers
528 and practical assessment of existing thermobarometers. J. Petrol. 31, 1353–1378.

529 Brey, G.P., Köhler, T.P., Nickel, K.G., 1990. Geothermobarometry in Four-phase Lherzolites I.
530 Experimental Results From 10 To 60 kb. J. Petrol. 31, 1313–1352.

531 Bussweiler, Y., Foley, S.F., Prelević, D., Jacob, D.E., 2015. The olivine macrocryst problem: New
532 insights from minor and trace element compositions of olivine from Lac de Gras kimberlites,
533 Canada. Lithos 220–223, 238–252. doi:10.1016/j.lithos.2015.02.016

534 Canil, D., 1999. The Ni-in-garnet geothermometer: Calibration at natural abundances. Contrib. to
535 Mineral. Petrol. 136, 240–246. doi:10.1007/s004100050535

536 Coogan, L.A., Saunders, A.D., Wilson, R.N., 2014. Aluminum-in-olivine thermometry of primitive
537 basalts: Evidence of an anomalously hot mantle source for large igneous provinces. Chem. Geol.
538 368, 1–10. doi:10.1016/j.chemgeo.2014.01.004

539 Creighton, S., Stachel, T., Matveev, S., Höfer, H., McCammon, C., Luth, R.W., 2009. Oxidation of the

Kaapvaal lithospheric mantle driven by metasomatism. Contrib. to Mineral. Petrol. 157, 491–504. doi:10.1007/s00410-008-0348-3

Day, H.W., 2012. A revised diamond-graphite transition curve. Am. Mineral. 97, 52–62. doi:10.2138/am.2011.3763

De Hoog, J.C.M., Gall, L., 2005. TRACE ELEMENT GEOCHEMISTRY OF MANTLE OLIVINE AND ITS APPLICATION TO GEOTHERMOMETRY. Ofioliti 20, 289–290.

De Hoog, J.C.M., Gall, L., Cornell, D.H., 2010. Trace-element geochemistry of mantle olivine and application to mantle petrogenesis and geothermobarometry. Chem. Geol. 270, 196–215. doi:10.1016/j.chemgeo.2009.11.017

Fedortchouk, Y., Canil, D., 2004. Intensive Variables in Kimberlite Magmas, Lac de Gras, Canada and Implications for Diamond Survival. J. Petrol. 45, 1725–1745. doi:10.1093/petrology/egh031

Foley, S.F., Prelevic, D., Rehfeldt, T., Jacob, D.E., 2013. Minor and trace elements in olivines as probes into early igneous and mantle melting processes. Earth Planet. Sci. Lett. 363, 181–191. doi:10.1016/j.epsl.2012.11.025

Gaul, O., Griffin, W., O'Reilly, S., Pearson, N., 2000. Mapping olivine composition in the lithospheric mantle. Earth Planet. Sci. … 182, 223–235.

Griffin, W.L., Cousens, D.R., Ryan, C.G., Sie, S.H., Suter, G.F., 1989. Ni in chrome pyrope garnets: a new geothermometer. Contrib. to Mineral. Petrol. 103, 199–202. doi:10.1007/BF00378505

Grütter, H., Latti, D., Menzies, A., 2006. Cr-saturation arrays in concentrate garnet compositions from kimberlite and their use in mantle barometry. J. Petrol. 47, 801–820. doi:10.1093/petrology/egi096

Grütter, H.S., 2009. Pyroxene xenocryst geotherms: Techniques and application. Lithos 112, 1167–1178. doi:10.1016/j.lithos.2009.03.023

562 Grütter, H.S., Gurney, J.J., Menzies, A.H., Winter, F., 2004. An updated classification scheme for mantle-
563 derived garnet, for use by diamond explorers. Lithos 77, 841–857. doi:10.1016/j.lithos.2004.04.012

564 Gurney, J.J., 1984. A correlation between garnets and diamonds in kimberlites., in: Kimberlite
565 Occurrence and Origin: A Basis for Conceptual Models in Exploration. pp. 143–166.

566 Harley, S.L., 1984. An experimental study of the partitioning of Fe and Mg between garnet and
567 orthopyroxene. Contrib. to Mineral. Petrol. 86, 359–373. doi:10.1007/BF01187140

568 Hasterok, D., Chapman, D.S., 2011. Heat production and geotherms for the continental lithosphere. Earth
569 Planet. Sci. Lett. 307, 59–70. doi:10.1016/j.epsl.2011.04.034

570 Howarth, G.H., Taylor, L.A., 2016. Multi-stage kimberlite evolution tracked in zoned olivine from the
571 Benfontein sill, South Africa. Lithos 262, 384–397. doi:10.1016/j.lithos.2016.07.028

572 Irvine, G.J., Graham Pearson, D., Kjarsgaard, B.A., Carlson, R.W., Kopylova, M.G., Dreibus, G., 2003. A
573 Re–Os isotope and PGE study of kimberlite-derived peridotite xenoliths from Somerset Island and a
574 comparison to the Slave and Kaapvaal cratons. Lithos 71, 461–488. doi:10.1016/S0024-
575 4937(03)00126-9

576 Jagoutz, E., Palme, H., Baddenhausen, H., Blum, K., Cendales, M., Dreibus, G., Spettel, B., Lorenz, V.,
577 Wänke, H., 1979. The abundances of major, minor and trace elements in the earth's mantle as
578 derived from primitive ultramafic nodules, in: Proc. Lunar Planet. Sci. Conf. 10th. pp. 2031–2050.

579 Kamenetsky, V.S., Kamenetsky, M.B., Sobolev, a. V., Golovin, a. V., Demouchy, S., Faure, K.,
580 Sharygin, V. V., Kuzmin, D. V., 2008. Olivine in the Udachnaya-East Kimberlite (Yakutia, Russia):
581 Types, Compositions and Origins. J. Petrol. 49, 823–839. doi:10.1093/petrology/egm033

582 Kennedy, C.S., Kennedy, G.C., 1976. The Equilibrium Boundary Between Graphite and Diamond. J.
583 Geophys. Res. 81, 2467–2470.

584 Kjarsgaard, B.A., Levinson, A.A., 2002. Diamonds in Canada. Gems Gemol. 38, 208–238.

585 Kjarsgaard, B.A., Peterson, T.D., 1992. Kimberlite-derived ultramafic xenoliths from the diamond
586 stability field : a new Cretaceous geotherm for Somerset Island , Northwest Territories. Curr. Res.
587 Part B. Pap. Geol. Surv. Can. 92–1B, 1–6.

588 Klemme, S., 2004. The influence of Cr on the garnet-spinel transition in the Earth's mantle: Experiments
589 in the system MgO-Cr2O3-SiO2 and thermodynamic modelling. Lithos 77, 639–646.
590 doi:10.1016/j.lithos.2004.03.017

591 Korolyuk, V.N., Pokhilenko, L.N., 2014. Electron probe determination of trace elements in olivine. X-
592 Ray Spectrom. 43, 353–358. doi:10.1002/xrs.2562

593 Mather, K., 2012. A Xenolith-Based Lithospheric Transect of the Slave Craton, NWT, Canada. Durham
594 University.

595 Mather, K.A., Pearson, D.G., McKenzie, D., Kjarsgaard, B.A., Priestley, K., 2011. Constraints on the
596 depth and thermal history of cratonic lithosphere from peridotite xenoliths, xenocrysts and
597 seismology. Lithos 125, 729–742. doi:10.1016/j.lithos.2011.04.003

598 Mckenzie, D., Bickle, M.J., 1988. The volume and composition of melt generated by extension of the
599 lithosphere. J. Petrol. 29, 625–679. doi:10.1093/petrology/29.3.625

600 McKenzie, D., Jackson, J., Priestley, K., 2005. Thermal structure of oceanic and continental lithosphere.
601 Earth Planet. Sci. Lett. 233, 337–349. doi:10.1016/j.epsl.2005.02.005

602 Milman-Barris, M.S., Beckett, J.R., Baker, M.B., Hofmann, A.E., Morgan, Z., Crowley, M.R., Vielzeuf,
603 D., Stolper, E., 2008. Zoning of phosphorus in igneous olivine. Contrib. to Mineral. Petrol. 155,
604 739–765. doi:10.1007/s00410-007-0268-7

605 Moore, A., Costin, G., 2016. Kimberlitic olivines derived from the Cr-poor and Cr-rich megacryst suites.

606 Lithos 258–259, 215–227. doi:10.1016/j.lithos.2016.04.022

607 Moore, A.E., 2012. The case for a cognate, polybaric origin for kimberlitic olivines. Lithos 128–131, 1–
608 10. doi:10.1016/j.lithos.2011.11.002

609 Nimis, P., Grütter, H., 2010. Internally consistent geothermometers for garnet peridotites and pyroxenites.
610 Contrib. to Mineral. Petrol. 159, 411–427. doi:10.1007/s00410-009-0455-9

611 Nimis, P., Taylor, W.R., 2000. Single clinopyroxene thermobarometry for garnet peridotites. Part I.
612 Calibration and testing of a Cr-in-Cpx barometer and an enstatite-in-Cpx thermometer. Contrib. to
613 Mineral. Petrol. 139, 541–554. doi:10.1007/s004100000156

614 Ringwood, A.E., 1966. Mineralogy of the mantle., in: Advances in Earth Science. p. 357.

615 Schulze, D.J., 1997. The significance of eclogite and Cr-poor megacryst Garnets in diamond exploration.
616 Explor. Min. Geol. 6, 349–366.

617 Sobolev, A. V, Hofmann, A.W., Kuzmin, D. V, Yaxley, G.M., Arndt, N.T., Chung, S.-L.S.-L.,
618 Danyushevsky, L. V, Elliott, T., Frey, F. a, Garcia, M.O., Gurenko, A. a, Kamenetsky, V.S., Kerr,
619 A.C., Krivolutskaya, N. a, Matvienkov, V. V, Nikogosian, I.K., Rocholl, A., Sigurdsson, I. a,
620 Sushchevskaya, N.M., Teklay, M., 2007. The amount of recycled crust in sources of mantle-derived
621 melts. Science (80-.). 316, 412–417. doi:10.1126/science.1138113

622 Spandler, C., O'Neill, H.S.C., 2010. Diffusion and partition coefficients of minor and trace elements in
623 San Carlos olivine at 1,300??C with some geochemical implications. Contrib. to Mineral. Petrol.
624 159, 1–28. doi:10.1007/s00410-009-0456-8

625 Stachel, T., Brey, G.P., Harris, J.W., 2005. Inclusions in Sublithospheric Diamonds: Glimpses of Deep
626 Earth. Elements 1, 73–78. doi:10.2113/gselements.1.2.73

627 Wan, Z., Coogan, L.A., Canil, D., 2008. Experimental calibration of aluminum partitioning between

olivine and spinel as a geothermometer. Am. Mineral. 93, 1142–1147. doi:10.2138/am.2008.2758

Ziberna, L., Klemme, S., Nimis, P., 2013. Garnet and spinel in fertile and depleted mantle: Insights from thermodynamic modelling. Contrib. to Mineral. Petrol. 166, 411–421. doi:10.1007/s00410-013-0882-5

Figure 1

Click here to download high resolution image

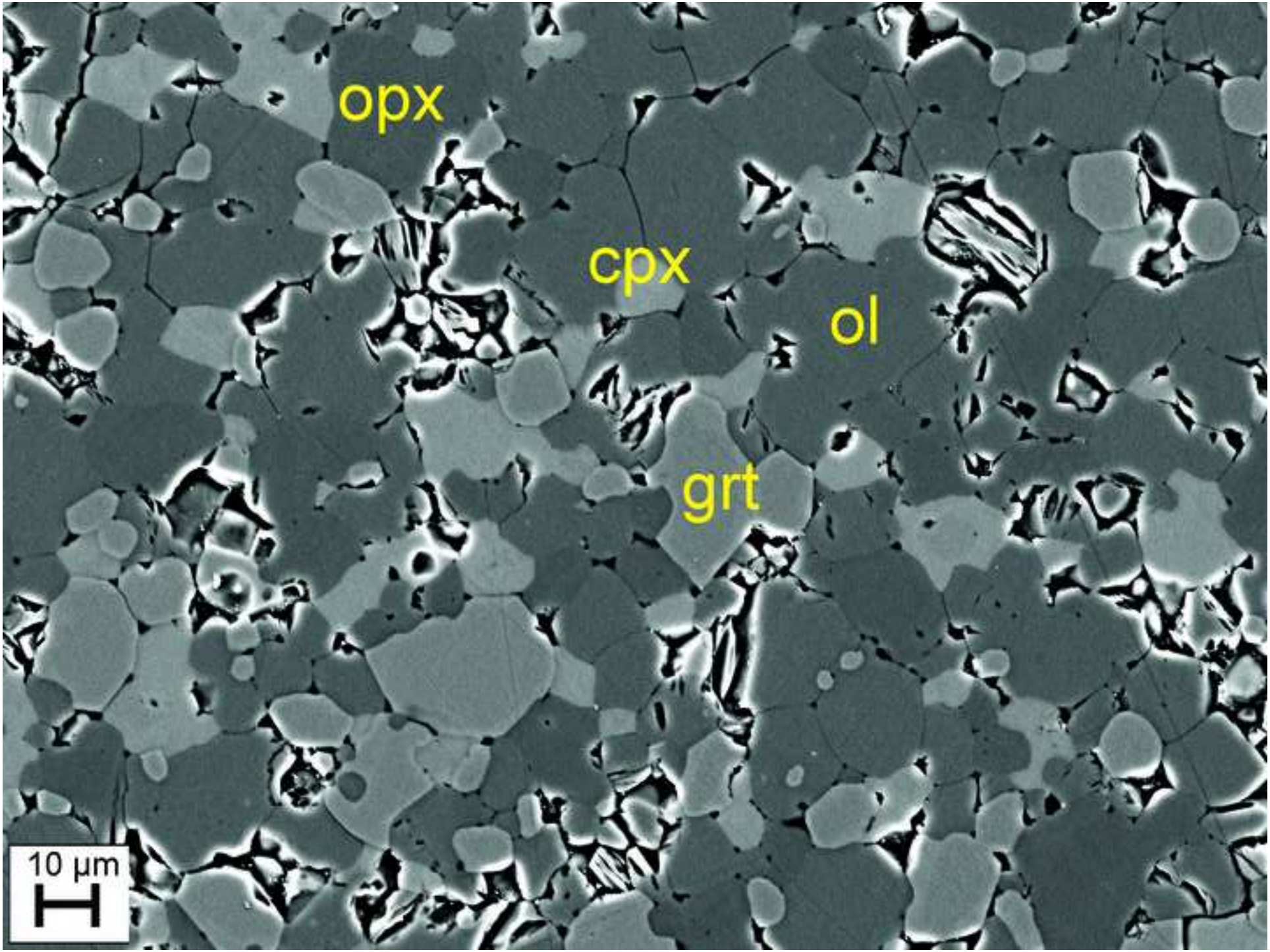

Figure 2

Click here to download high resolution image

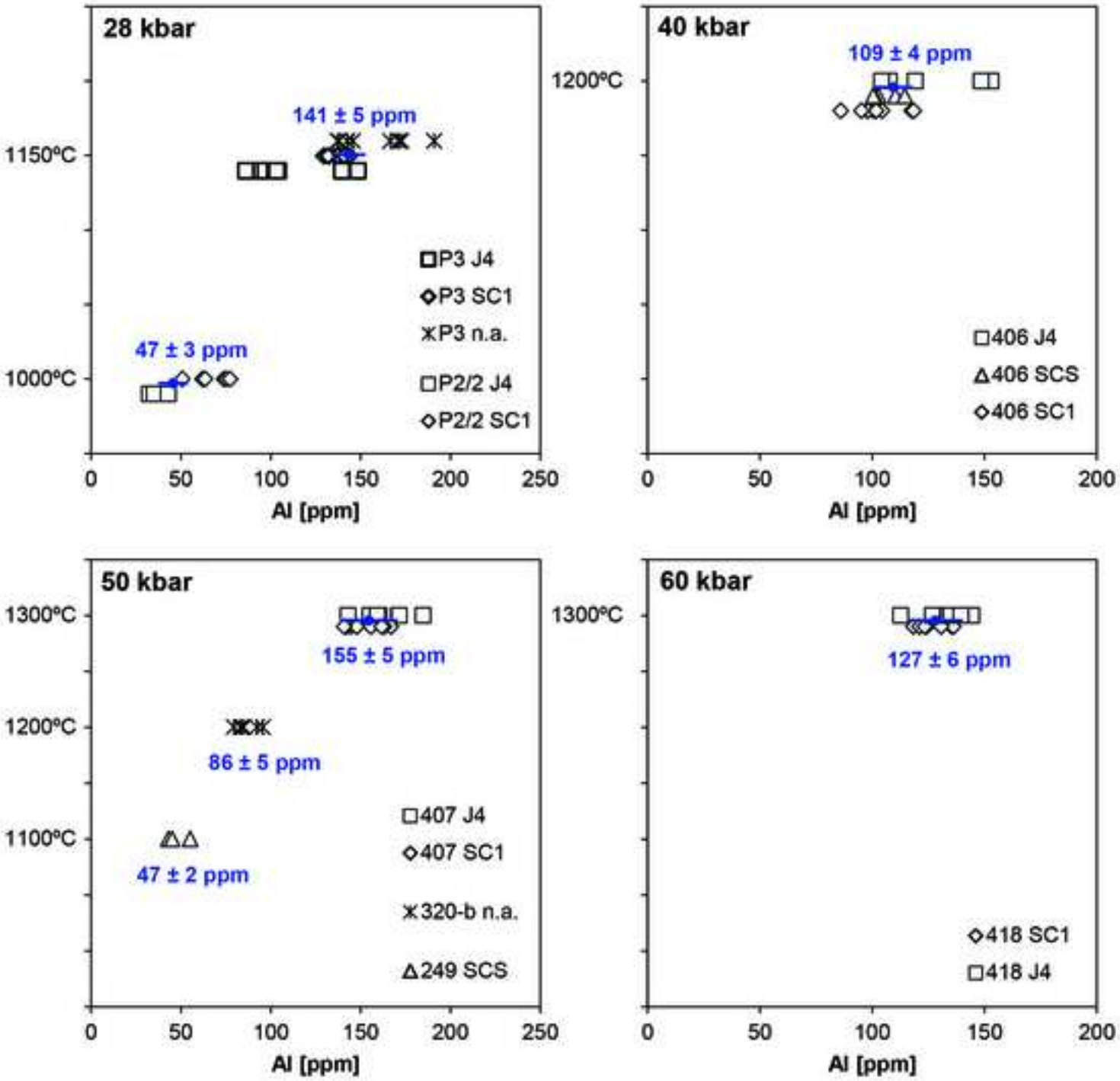

Figure 3

Click here to download high resolution image

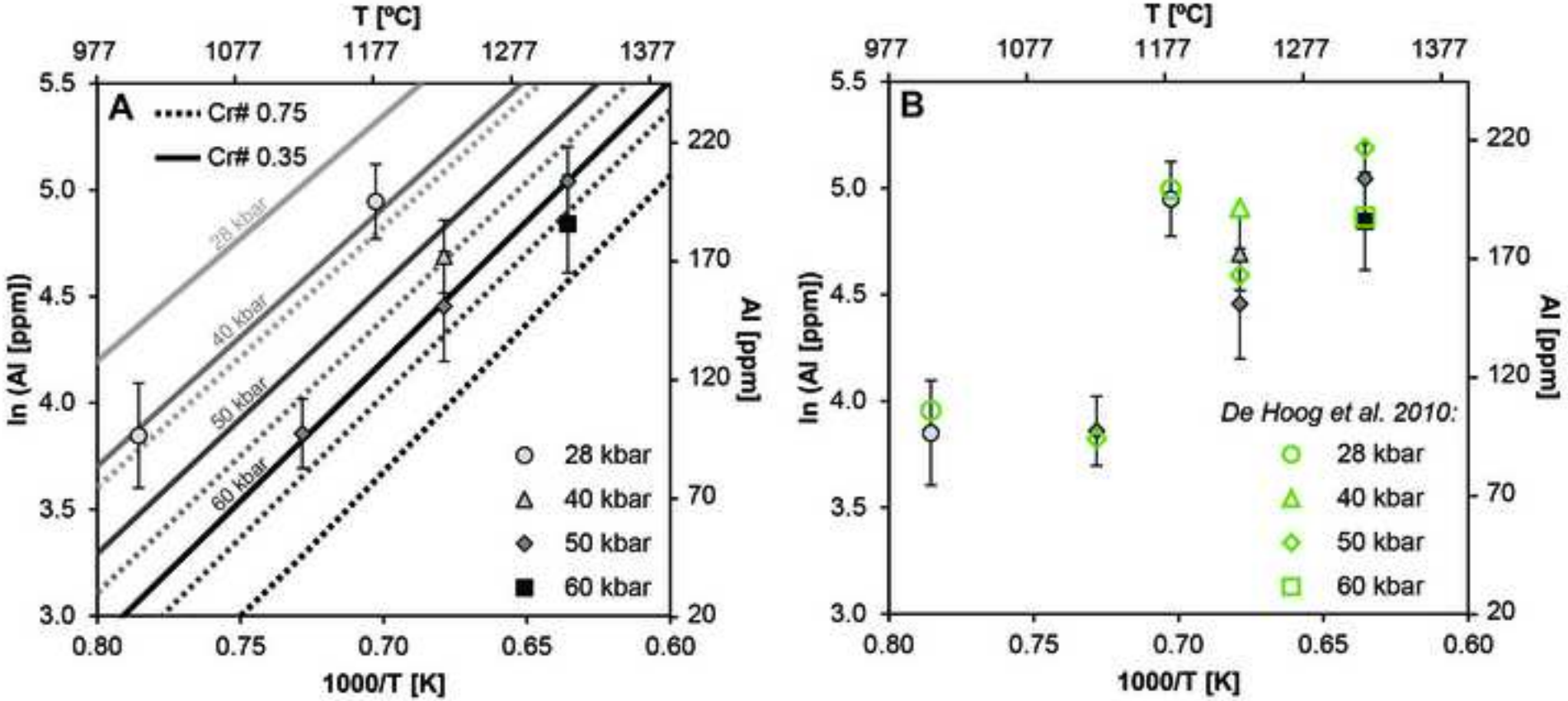

Figure 4

Click here to download high resolution image

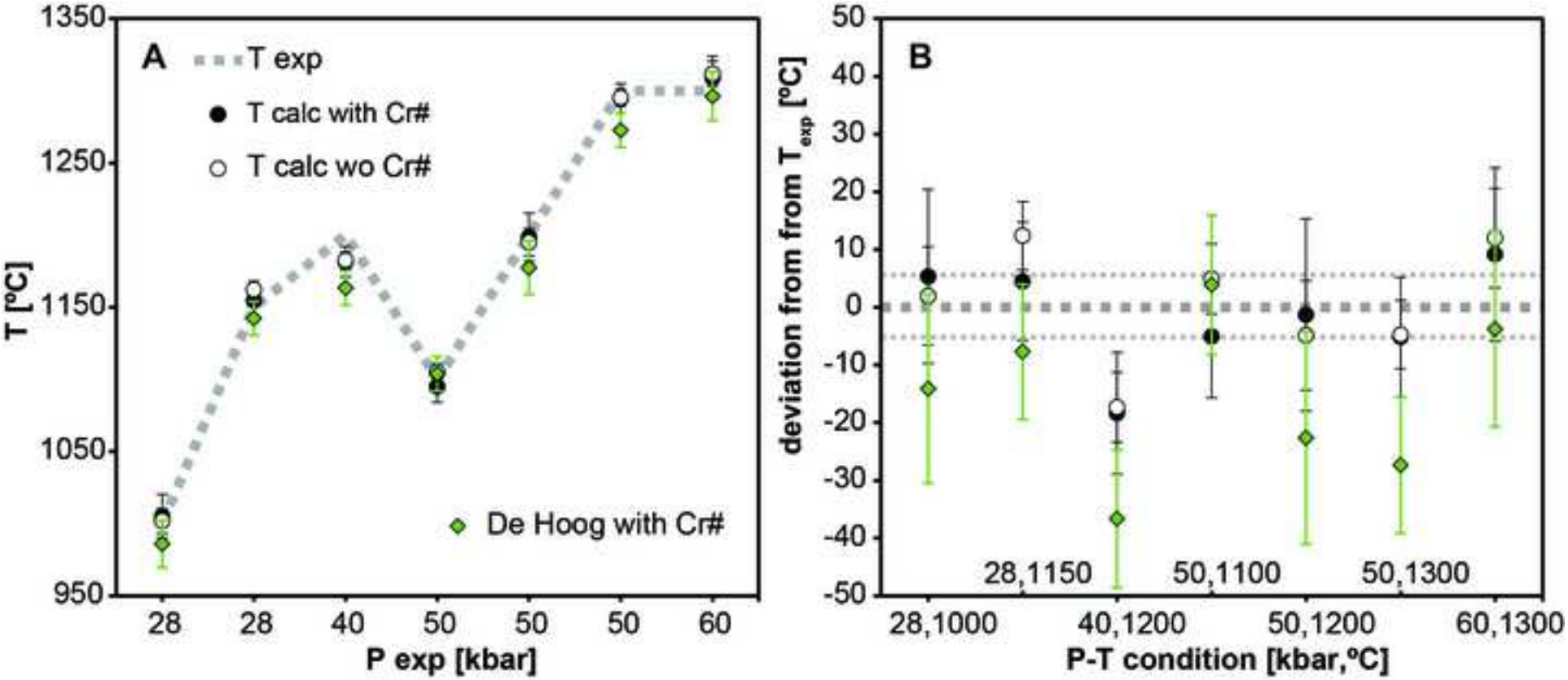

Figure 5

Click here to download high resolution image

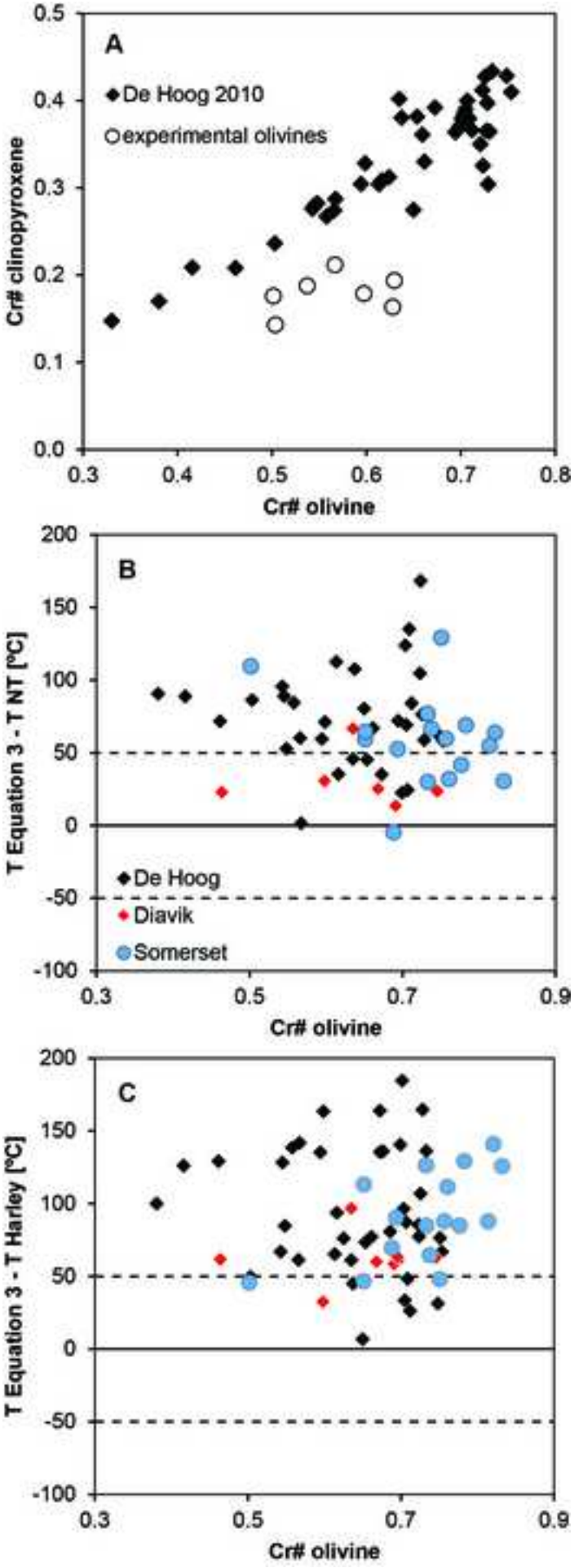

Figure 6

Click here to download high resolution image

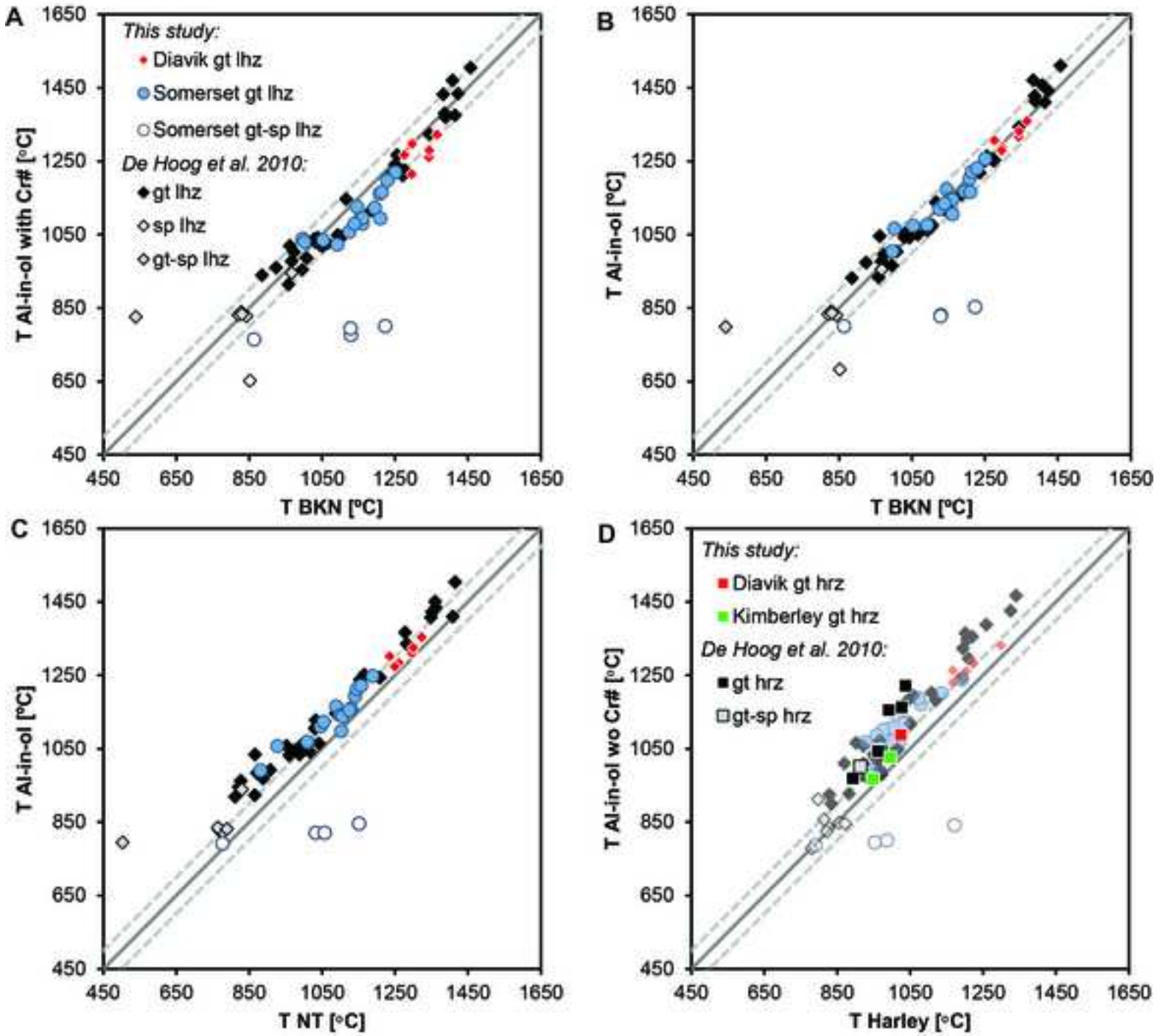

Figure 7

Click here to download high resolution image

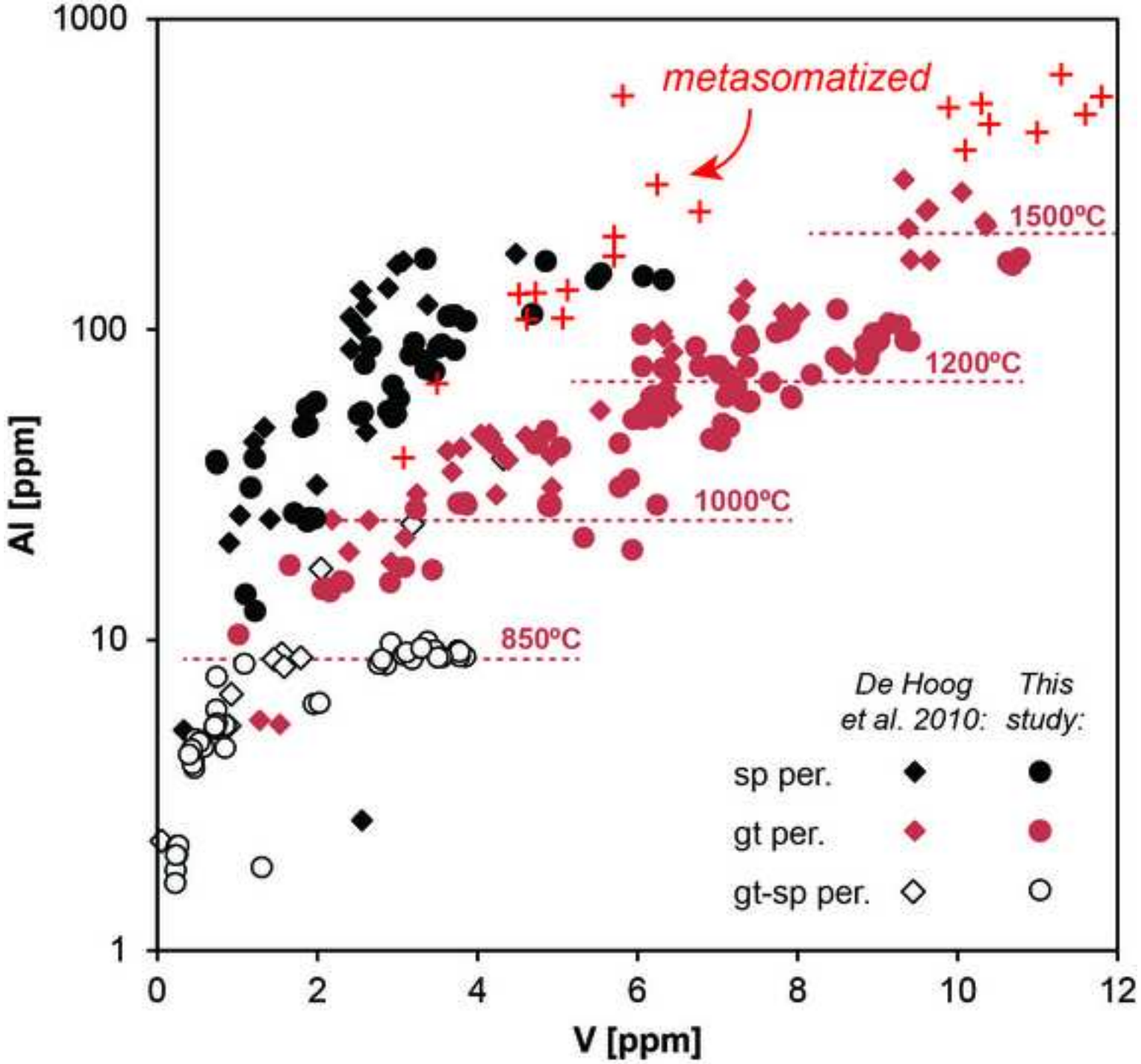

Figure 8

Click here to download high resolution image

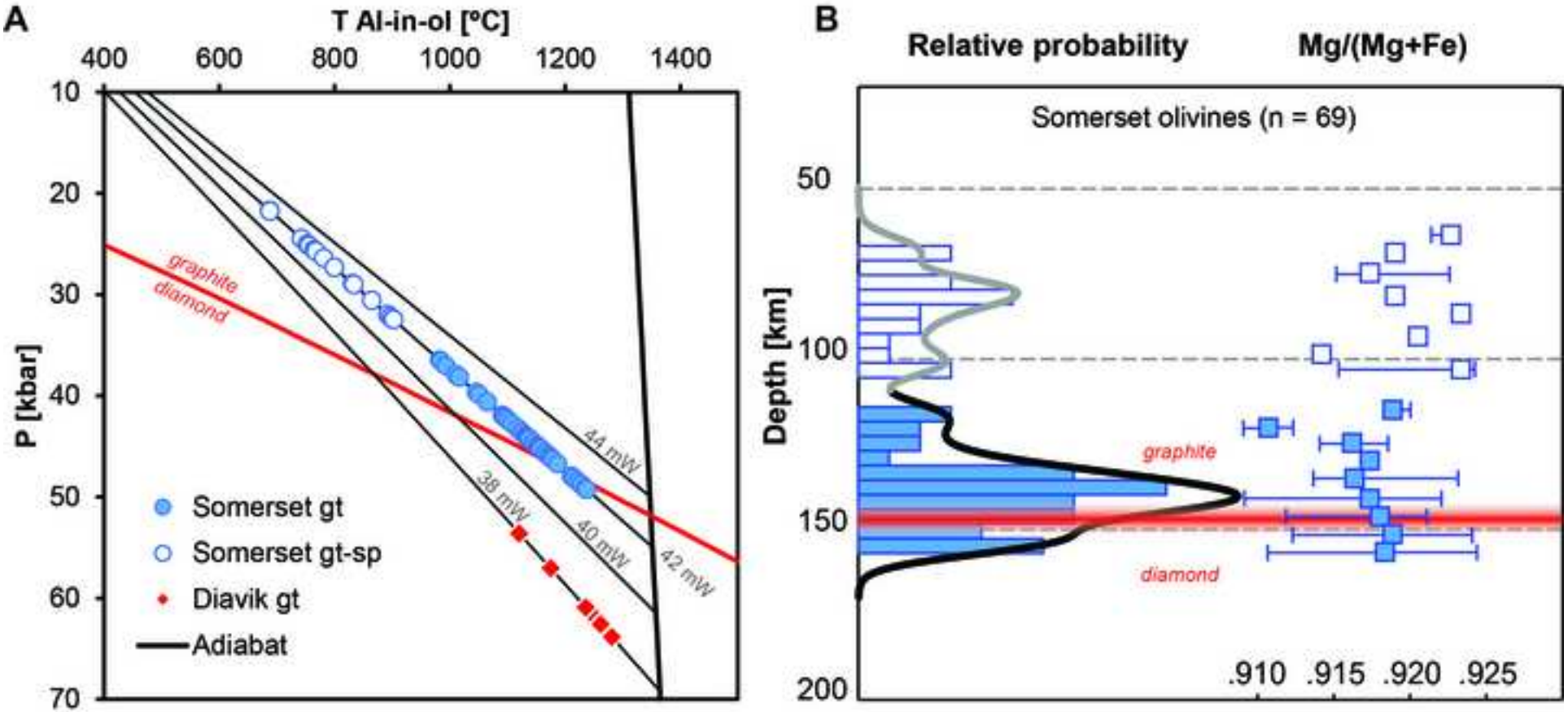

Table 1
Click here to download Table: Table 1.xlsx

Table 1: List of samples with original lables by Brey et al. (1990) and newly adopted lables in this s

	Brey et al. (1990)			
Run	**P [kb]**	**T [ºC]**	**Starting**	**SEM**
P2/2	28	1000	J4	m1336_A
			SC1	m1336_B
P3	28	1150	J4	m1332_A
			SC1	m1332_B
			n.a.*	m1332_C
406	40	1200	SC1	m1334_A
			SCS	m1334_B
			J4	m1334_C
249	50	1100	SCS	m1329_C
320b	50	1200	n.a.*	m1330_D
407	50	1300	J4	m1337_A
			SC1	m1337_B
418	60	1300	J4	m1340_A
			SC1	m1340_B

*Starting material could not be reliably identified.

Table 2
Click here to download Table: Table 2.xlsx

Table 2: Al concentrations in experimental olivines measured by SIMS (screened for contamination)

Brey et al. (1990)				*This study*			
Run	**P [kb]**	**T [ºC]**	**Starting Material**	**SIMS sample ID**	**Measuring point**	**Al [ppm]**	**2σ [ppm]**
P2/2	28	1000	J4	S3331A	S3331A_OL_1	42	2
					S3331A_OL_2	40	1
					S3331A_OL_3	41	1
					S3331A_OL_4	42	1
					S3331A_OL_6	33	1
					S3331A_OL_7	35	1
					S3331A_OL_8	43	2
			SC1	S3331B	S3331B_OL_1	74	3
					S3331B_OL_2	75	5
					S3331B_OL_3	63	2
					S3331B_OL_4	62	2
					S3331B_OL_5	77	7
					S3331B_OL_7	51	3
					S3331B_OL_8	63	3
P3	28	1150	J4	S3321A	S3321A_OL_1	102	4
					S3321A_OL_3	104	3
					S3321A_OL_4	149	5
					S3321A_OL_5	94	3
					S3321A_OL_6	89	3
					S3321A_OL_7	86	3
					S3321A_OL_8	140	5
					S3321A_OL_9	103	3
			SC1	S3321B	S3321B_OL_1	136	5
					S3321B_OL_3	138	5
					S3321B_OL_4	133	5
					S3321B_OL_5	130	5
					S3321B_OL_6	132	4
					S3321B_OL_8	144	5
					S3321B_OL_9	141	5
			n.a.*	S3321C	S3321C_OL_1	146	7
					S3321C_OL_2	143	5
					S3321C_OL_3	138	5
					S3321C_OL_4	173	6
					S3321C_OL_5	171	6
					S3321C_OL_7	191	6
					S3321C_OL_8	171	6
					S3321C_OL_10	167	5
					S3321C_OL_11	137	5
					S3326A_OL_1	98	3
					S3326A_OL_2	118	5
					S3326A_OL_3	119	5
					S3326A_OL_5	104	4

Table 3
Click here to download Table: Table 3.xlsx

Table 3: Equilibrium Al values and Cr# for the different experimental runs

Run	P [kb]	T [ºC]	Al [ppm]	2σ [ppm]	Cr#*
P2/2	28	1000	47	3	0.63
P3	28	1150	141	5	0.60
406	40	1200	109	4	0.56
249	50	1100	47	2	0.63
320b	50	1200	86	5	0.53
407	50	1300	155	5	0.50
418	60	1300	127	6	0.50

*Calculated with average Cr concentrations from the habilitation thesis of Brey (1989).

Table 4
Click here to download Table: Table 4.xlsx

Table 4: Mineral compositions for mantle xenolith samples from Diavik and Somerset Island kimberlites and thern

Location	Diavik	Diavik	Diavik	Diavik	Diavik	Diavik	Diavik
Sample	DDM_327	DDM_360	DDM_367A	DDM_368	DDM_335	DDM_366	MX5023
Type	gt lhz	gt lhz	gt lhz	gt lhz	gt lhz	gt lhz	gt hrz
Major and minor element analyses by EPMA (wt%) [a)]							
Olivine							
Na_2O	-	0.00	0.00	0.00	0.00	0.00	0.01
CaO	0.05	0.04	0.05	0.04	0.05	0.05	0.02
FeO	9.25	8.98	8.70	8.49	8.70	8.69	7.21
SiO_2	41.5	41.2	40.8	41.3	40.8	41.3	42.0
K_2O	-	0.00	0.00	0.00	0.00	0.00	0.01
MgO	50.3	50.8	50.5	51.0	50.6	50.6	50.1
TiO_2	0.02	0.01	0.02	0.01	0.02	0.02	0.00
Cr_2O_3	0.04	0.02	0.05	0.04	0.05	0.05	0.03
MnO	0.13	0.12	0.12	0.10	0.12	0.12	0.08
NiO	0.39	0.43	0.38	0.40	0.38	0.39	0.34
Total	101.7	101.6	100.6	101.4	100.7	101.2	99.8
Trace elements in olivine measured by LA-ICP-MS (ppm) [b)]							
Al	95	82	61	81	79	88	47
V	9.08	7.35	7.93	7.51	8.70	8.89	7.05
Cr#	0.60	0.46	0.75	0.64	0.69	0.67	0.70
Orthopyroxene							
Na_2O	-	0.00	0.00	0.00	0.00	0.00	0.11
CaO	0.99	0.80	0.79	0.77	0.91	0.92	0.61
Al_2O_3	0.71	0.64	0.59	0.60	0.67	0.68	0.51
FeO	5.72	5.44	5.36	5.18	5.22	5.25	4.37
SiO_2	58.4	58.6	57.8	58.1	57.5	58.0	58.5
K_2O	-	0.00	0.00	0.00	0.00	0.00	0.01
MgO	35.1	35.5	35.6	35.9	35.3	35.1	35.5
TiO_2	0.13	0.06	0.12	0.07	0.13	0.12	0.06
Cr_2O_3	0.22	0.17	0.38	0.35	0.34	0.33	0.31
MnO	0.13	0.12	0.13	0.12	0.13	0.13	0.17
NiO	0.14	0.13	0.12	0.12	0.11	0.13	0.00
Total	101.5	101.5	100.9	101.2	100.3	100.7	100.1
Clinopyroxene							
Na_2O	1.42	1.37	1.47	1.44	1.51	1.50	-
CaO	17.8	18.9	18.8	19.1	17.9	17.8	-
Al_2O_3	1.72	1.75	1.38	1.44	1.61	1.60	-
FeO	3.48	3.13	2.97	2.79	3.08	3.06	-
SiO_2	55.9	56.3	55.3	55.7	55.2	55.1	-
K_2O	0.06	0.05	0.06	0.05	0.04	0.04	-
MgO	19.3	19.0	18.7	18.6	19.0	19.0	-
TiO_2	0.22	0.11	0.18	0.11	0.21	0.20	-